Contemporary Mathematics
Volume 180, 1994

Direct Numerical Simulation of Jet Flow via a Multi-block Technique

H. C. Ku, H. E. Gilreath, R. Raul and J. C. Sommerer

Abstract

A multi-grid domain decomposition approach by the pseudospectral element method is used to simulate a two-dimensional jet emanating from the nozzle. The solution technique is to implement the Schwarz alternating procedure for exchanging data among subdomains, where the coarse-grid correction is used to remove the high frequency error.

Numerical results of jet flow not only provide the possible mechanism of turbulence formation, but also quantitatively capture all the phenomena for flow transition from the laminar to the turbulent structure.

1 Introduction

Turbulence, a phenomenon related to but distinct from chaos, has been increasingly in the focus of physics research in a variety of flows for the last two decades. Although there is no unique mathematical model that encompasses all flow environments, it is possible to gain an insight into turbulence through direct numerical simulation (low Reynolds numbers). In order to model all the features of turbulence, one needs to resolve the smallest length scale, i.e., the Kolmogorov length scale at which the turbulent energy carried from the large length scales is dissipated into heat by the molecular viscosity. Based on the Kolmogorov dissipation scale, the ratio of length scales in one dimension is estimated as the reciprocal of $Re^{\frac{3}{4}}$. Thus, in the Kolmogorov theory of three-dimensional turbulent flow, there are at least on the order $Re^{\frac{9}{4}}$ dynamically active degrees of freedom for a given volume.

A special device is used to simulate the two-dimensional turbulence of jets by imposing a strong stratification along the vertical direction, so that the resulting

1991 Mathematics Subjet Classification. Primary 65N35, 68Q10; Secondary 76D05
This work was partially supported by the SPAWAR under the Contract N00039-91-C-0001.
This paper is in final form and no version of it will be submitted for publication elsewhere.

0271-4132/94 $1.00 + $.25 per page

flow occurs mainly in a horizontal plane. This allows the direct numerical simulation to be performed on the HP9000/735 work station machine.

To address the goal of the direct numerical simulation of turbulent flow, the desired features of numerical algorithms are: (1) applicability to a variety of geometrical shapes; (2) high resolution in steep gradient areas (multi-grid or single-grid technique); (3) minimal working space (domain decomposition); and (4) low running time of computation (multiple processors). A novel pseudospectral element method [1] that contains the above mentioned features is ideally suitable for the proposed work.

2 Navier-Stokes Equations

For an incompressible flow, the time-dependent Navier-Stokes equations are:

$$\frac{\partial \mathbf{u}}{\partial t} + \mathbf{u} \cdot \nabla \mathbf{u} = -\nabla p + \frac{1}{Re} \nabla^2 \mathbf{u}, \tag{1a}$$

$$\nabla \cdot \mathbf{u} = 0. \tag{1b}$$

Here $\mathbf{u}$ is the velocity vector, p the pressure, $\mathrm{Re} = UL/\nu$ the Reynolds number (U, L the characteristic velocity and length, respectively), and ν the kinematic viscosity.

To simplify the notation while explaining the basic ideas, we write the equations as if we could compute exact spatial derivatives in the curvilinear coordinates. The method utilized to solve the Navier-Stokes equations is fourth-order Runge-Kutta time integration scheme based on the Chorin's [2] splitting technique. According to this scheme, the equations of motion read

$$\frac{\partial u_i}{\partial t} + \frac{\partial p}{\partial x_i} = F_i \tag{2}$$

where $F_i = -u_j \partial u_i / \partial x_j + 1/Re \partial^2 u_i / \partial x_j^2$.

At each stage, the first step is to split the velocity into a sum of predicted and corrected values. The predicted velocity is determined by time integration of momentum equations without the pressure term and the second step develops pressure and corrected velocity fields that satisfy the continuity equation.

1st stage:
$$\bar{u}_i^1 = u_i^n + \frac{\Delta t}{2} F_i(u_i^n) \tag{3a}$$

$$u_i^1 = \bar{u}_i^1 - \frac{\Delta t}{2} \frac{\partial p}{\partial x_i}, \quad \frac{\partial u_i^1}{\partial x_i} = 0; \tag{3b}$$

2nd stage:
$$\bar{u}_i^2 = u_i^n + \frac{\Delta t}{2} F_i(u_i^1) \tag{4a}$$

$$u_i^2 = \bar{u}_i^2 - \frac{\Delta t}{2} \frac{\partial p}{\partial x_i}, \quad \frac{\partial u_i^2}{\partial x_i} = 0; \tag{4b}$$

3rd stage:
$$\bar{u}_i^3 = u_i^n + \Delta t F_i(u_i^2) \tag{5a}$$

$$u_i^3 = \bar{u}_i^3 - \Delta t \frac{\partial p}{\partial x_i}, \quad \frac{\partial u_i^3}{\partial x_i} = 0; \quad \text{and} \tag{5b}$$

4th stage:
$$\bar{u}_i^{n+1} = u_i^n + \Delta t \left\{ \frac{F_i(u_i^n)}{6} + \frac{F_i(u_i^1)}{3} + \frac{F_i(u_i^2)}{3} + \frac{F_i(u_i^3)}{6} \right\} \tag{6a}$$

$$u_i^{n+1} = \bar{u}_i^{n+1} - \Delta t \frac{\partial p}{\partial x_i}, \quad \frac{\partial u_i^{n+1}}{\partial x_i} = 0. \tag{6b}$$

The main features of this method include: (i) for a given accuracy the time step size is larger than that of the first-order scheme and (ii) the most promising time integration scheme conserves the total energy during the evolution of inviscid flow [1]. The approach is very effective for flow at high Reynolds numbers because the gain in time step size offsets more than the cost of four pressure solvers.

At each stage, the pressure Poisson equation can be generated by taking the divergence operator of the corrected velocity. In the Cartesian coordinates a direct solution of pressure equation can be obtained by the eigenfunction expansion technique [3], while in the curvilinear coordinates the pressure solution is governed by the iterative preconditioned minimal residual method [1].

3 Domain Decomposition with Multi-Grid SAP

The SAP iterative scheme has been successfully applied to those configurations where the overlapped grids coincide with each other [3]. Under this condition, which we call the single-grid SAP, no data interpolation error occurs. The success of the single-grid SAP lies in the exclusive use of the continuity equation as the pressure boundary condition in the overlapping area, and the velocity difference in the overlapping area is reduced by one order of magnitude after each SAP iteration. Under some circumstances, the overlapped grid positions may not coincide with each other due to the complexity of the geometrical configuration, as in a submarine or automobile, where there arises a need for a possible layout of mixed grids or the application of adaptive fine grids in one subdomain to resolve steep changes of variables. But simply exchanging the data through interpolation in the inter-overlapping areas will cause high-frequency error and pollute the results throughout the whole computational domain [4].

The multi-grid technique, which has long been advocated by finite-difference users [5], employs a sequence of grids to accelerate the convergence of iterative methods. The work rests on "standard coarsening," i.e., doubling the mesh in each direction from one grid to the next coarsest grid. The problem is solved on the coarse grid, and the coarse-grid correction is recursively transferred back to the fine grid to obtain rapid convergence. It can apply to the overlapping area as well [5].

In addition to the Lagrangian constraint between the pressure and velocity field, the noncoinciding overlapped grids (nonequal-spaced collocation points) in the inter-overlapping areas enhance the difficulty of applying the multi-grid technique. However, the idea of "coarse-grid correction" is still effective in reducing high-frequency error. The strategy behind the coarse-grid correction process is to adopt the idea proposed by Thompson and Ferziger [6], modified as

$$\nabla_c \cdot \mathbf{u}_c - \nabla_c \cdot (I_c^f \mathbf{u}_f) = I_c^f (r_f - \nabla_f \cdot \mathbf{u}_f). \tag{7}$$

Here $\nabla_c \cdot$ represents the operator of divergence on the coarse-grid subdomain. I_c^f is an interpolation operator from the fine-grid subdomain "f" to coarse grid subdomain "c", and $\mathbf{u}$ is the velocity. r_f is simply the result of the divergence of the velocity field which should be set to zero. The left-hand side of Eq. (7) is the difference between the coarse-grid operator acting on the coarse-grid subdomain and the coarse-grid operator acting on the interpolated fine-grid subdomain (which is held fixed). When substituting the coarse-grid velocity in terms of pressure gradient (Eqs. (3 - 6)), the first term on the-left hand side of Eq. (7) becomes the pressure equation acting on the coarse-grid subdomain, while the right-hand side of Eq. (7)

is the interpolated residual of $\nabla \cdot \mathbf{u}$ from the fine-grid subdomain. It is apparent that once the solution of the fine-grid subdomain has been found the residual will be zero (exactly satisfy the pressure Poisson equation), which implies

$$\mathbf{u}_c = I_c^f \mathbf{u}_f. \tag{8}$$

When the residual is non-zero, Eq. (7) acts as a forcing term for the coarse-grid correction and transfers the correction of $\mathbf{u}$ back to the fine-grid subdomain, i.e.,

$$\mathbf{u}_f^{new} = \mathbf{u}_f^{old} + I_f^c(\mathbf{u}_c - I_c^f \mathbf{u}_f^{old}). \tag{9}$$

This is vital for the success of the scheme. Changes in the velocity field are transferred back to the fine-grid subdomain rather than the velocity field itself. Meanwhile, the error index, ℓ_2 norm of $\omega = \| \mathbf{u}_c - \mathbf{I}_c^f \mathbf{u}_f \|$, provides a good monitor for the evolution of the flow field. Any unexpected increase in ω reflects that an extremely steep change of flow field occurs in the overlapping area, otherwise, the error index ω should remain in the same range of order of magnitude. Notice that when the overlapped grids in the overlapping areas are coinciding with each other, the interpolation operator I_c^f becomes a unitary matrix.

The multi-grid domain decomposition technique for the direct numerical simulation of jet flow sketched in Fig. 1 is summarized by the following algorithm:

1. First set $\mathbf{u}^{n+1}$ on $\overline{AB}, \overline{CD}, \overline{EF}, \overline{GH}$. Usually $\mathbf{u}^n$ will be a good initial guess.
2. Solve the fine-grid domain III employing the boundary conditions derived from the continuity equation on $\overline{AB}, \overline{CD}$, where the pressure solution is directly obtained by the eigenfunction expansion technique. While in domain I with the same type of boundary condition for the pressure on $\overline{EF}, \overline{GH}$, the iterative preconditioned method is used to get the pressure solution.
3. With the interpolated $\mathbf{u}^{n+1}$ from step (2) on domain III $\cap$ IV, solve the coarse-grid domain IV to update $\mathbf{u}^{n+1}$ on domain III $\cap$ IV by the coarse-grid correction process. With the velocity $\mathbf{u}^{n+1}$ along $\overline{IJ}, \overline{KL}$ from domain I & III, a single grid method is to give the pressure solution for domain II.
4. Repeat steps (2) & (3) until the error index ω among the overlapping areas meets the convergence criterion.

4 Results and discussion

In the interest of brevity, no effort is made hereafter in this paper to discuss the turbulent quantities, the fluctuation velocity (u_i') and turbulent stresses ($\overline{u_i' u_j'}$). However, they can be derived from the mean velocity (temporal average based on every time interval), i.e., $u_i' = u_i - \bar{u}_i$, and $\overline{u_i' u_j'} = \overline{u_i u_j} - \bar{u}_i \bar{u}_j$.

In order to make a comparison with the results obtained by the experiment, a realistic experimental scale of will be used by the direct numerical simulation. A slit of 0.1 inch wide is designed as the narrow part of a round nozzle whose diameter is 0.125 inch. A jet flow is discharged into a stratified tank with 1.5 feet wide and 1.5 feet long, and the upstream of a nozzle is connected by a 6 inch wide reservoir in which the fluid is driven by a constant moving piston.

As illustrated in Fig. 1, the computational domain is decomposed into four subdomains with overlapping areas: the upstream reservoir where a constant moving

piston is used to drive the flow, the convergent nozzle where the incoming flow from the reservoir is developed to gain a high speed, the immediate downstream from the entrance of the nozzle where the high speed jet is discharged into the tank, and the far downstream area where a well-developed turbulent flow can be traced. In order to resolve the Kolmogorov length scale in the interesting area (indicated by the fine grid distribution), for the case of $Re = 500$, the number of points (element layout as plotted in Fig. 2) applied to each subdomain is 61 × 79 for domain I, 61 × 31 for domain II, 115 × 151 for domain III, and 97 × 139 for domain IV, separately.

Figs. 3 depict the streamline plot of jet flow at Re = 500. During the time evolution of jet flow, the symmetry of jet front will not be distorted at the early stage (laminar flow as seen in Fig. 3a) until the phase speed of the vortex shedding (due to flow instability) travels faster than that of jet front. Fig. 3b shows the onset of vortex shedding and Fig. 3c demonstrates that the jet front is not symmetric any more. A pair of vortices adjacent to the jet front represents the extrusion of the jet into the ambient fluid. Once the jet front is caught up by the incoming travelling waves, the energy transferred by the vortex shedding, in a cascade process from the highest at the nozzle exit (high shedding frequency) to the lowest at the jet front (low shedding frequency), splits into two parts: one for the jet front pushing against the ambient viscous fluid, and another travelling back, causing a wave-wave interaction. Initially, the wave-wave interaction starts close to the jet front and gradually propagates backward toward the nozzle exit. This process constitutes a complete mechanism to account for the turbulent formation. The longer the elapsed time, the more unstable the flow becomes. Fig. 3d gives a clear picture of flow development (nearly turbulent) at a longer time. A few distinct pairs of vortices always exist within 1 to 5 inches of the nozzle exit, the appearance of which are also confirmed by an APL Fluid Dynamics Laboratory experiment.

References

[1] H. C. Ku, A. P. Rosenberg and T. D. Taylor, *in the 12th Intl. Conference on numerical Methods in Fluid Dynamics*, Proceedings, Oxford, 1990, Lecture Notes in Physics, Springer-Verlag, 223-227.

[2] A. J. Chorin, "Numerical Solution of Navier-Stokes Equations," *Math. Comp.* **22** (1968), 745-762.

[3] H. C. Ku, R. S. Hirsh, T. D. Taylor and A. P. Rosenberg, "A Pseudospectral Matrix Element Method for Solution of Three-Dimensional Incompressible Flows and Its Parallel Implementation," *J. Comput. Phys.* **83** (1989), 260-291.

[4] H. C. Ku and B. Ramaswamy, *in the 6th Copper Mountain Conference on Multigrid Methods*, NASA Conference Publication (edited by N. D. Melson et al.), Colorado (1993), 293-304.

[5] W. Hackbusch, "Multi-Grid Methods and Applications," Springer-Verlag, Berlin, (1985).

[6] M. C. Thompson and J. H. Ferziger, "An Adaptive Multigrid Technique for the Incompressible Navier-Stokes Equations," **82** (1989), 94-121.

Johns Hopkins University Applied Physics Laboratory, Laurel, Maryland 20723

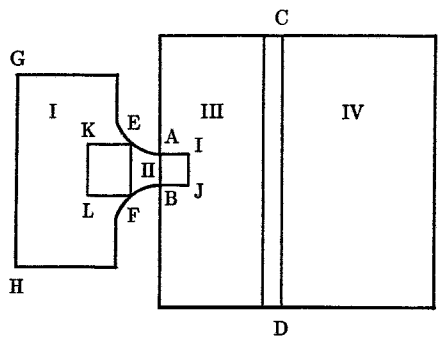

Figure 1: Configuration of domain decomposition for jet flow

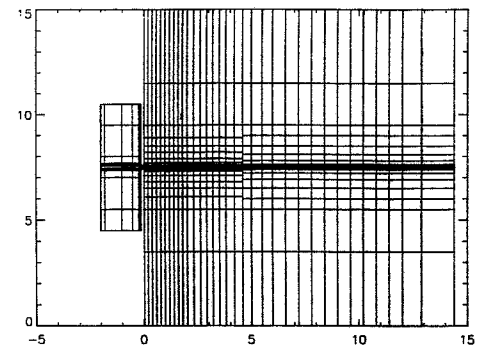

Figure 2: Element layout of jet flow (6 × 6 points per element)

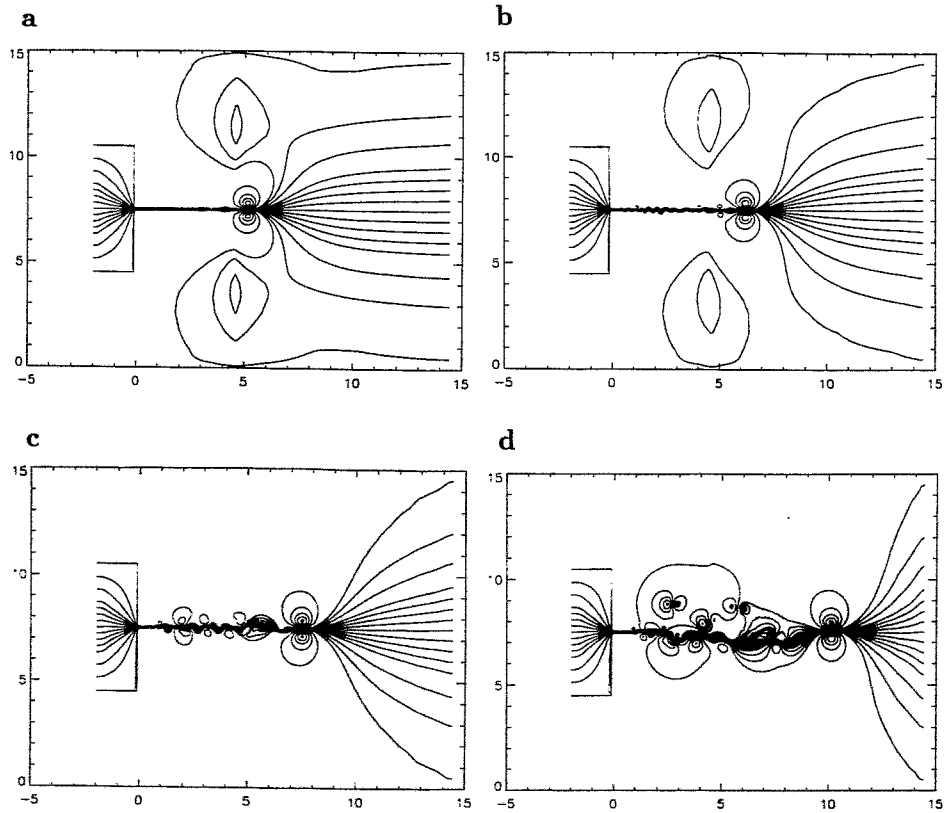

Figure 3: Streamline plots for Re = 500 at time (a) t = 120, (b) t = 150, (c) t = 180, and (d) t = 255.